J MATER RES TECHNOL. 2020;9(4):9016–9028

Available online at www.sciencedirect.com

jmr&t Journal of Materials Research and Technology

www.jmrt.com.br

Original Article

Estimating strength properties of geopolymer self-compacting concrete using machine learning techniques

Paul O. Awoyera[a,b,c,*], *Mehmet S. Kirgiz*[d], *A. Viloria*[e,f], *D. Ovallos-Gazabon*[g]

[a] *Department of civil Engineering, Covenant University, Ota, Nigeria*
[b] *Institute of Research and Development, Duy Tan University, Da Nang 550000, Vietnam*
[c] *Faculty of Civil Engineering, Duy Tan University, Da Nang 550000, Vietnam*
[d] *Instanbul University-Cerrahpasa, 34320 Avcilar, Instanbul, Turkey*
[e] *Universidad de la Costa, Barranquilla, Colombia*
[f] *Universidad peruana de ciencias aplicadas, lima, Peru*
[g] *Universidad Simon Bolivar, Barranquilla, Colombia*

ARTICLE INFO

Article history:
Received 23 April 2020
Accepted 3 June 2020
Available online 24 June 2020

Keywords:
Artificial neural networks
Genetic programming
Predictor
Response
Self-Compacting concrete
Geopolymers

ABSTRACT

There has been a persistent drive for sustainable development in the concrete industry. While there are series of encouraging experimental research outputs, yet the research field requires a standard framework for the material development. In this study, the strength characteristics of geopolymer self-compacting concrete made by addition of mineral admixtures, have been modelled with both genetic programming (GEP) and the artificial neural networks (ANN) techniques. The study adopts a 12M sodium hydroxide and sodium silicate alkaline solution of ratio to fly ash at 0.33 for geopolymer reaction. In addition to the conventional material (river sand), fly ash was partially replaced with silica fume and granulated blast furnace slag. Various properties of the concrete, filler ability and passing ability of fresh mixtures, and compressive, split-tensile and flexural strength of hardened concrete were determined. The model development involved using raw materials and fresh mix properties as predictors, and strength properties as response. Results shows that the use of the admixtures enhanced both the fresh and hardened properties of the concrete. Both GEP and ANN methods exhibited good prediction of the experimental data, with minimal errors. However, GEP models can be preferred as simple equations are developed from the process, while ANN is only a predictor.

* *Corresponding author at*: Department of Civil Engineering, Covenant University, Ota, Nigeria.
E-mail: awopaul2002@gmail.com (P.O. Awoyera).

https://doi.org/10.1016/j.jmrt.2020.06.008

1. Introduction

On yearly basis, emission of greenhouse gases (CO_2 and NOx) during cement production is about 1.6 billion tons [1,2]{Merging Citations}. The biodiversity and environment are largely affected by the hazardous greenhouse gases, dust dispersion, particulate matter emissions, and many others effects [3,4]. For these reasons, other form of concrete involving no use of Portland cement and other new construction materials and technologies has been developed [5–7]. Cementation in such mixture matrix is achieved using geopolymer materials.

The amount of harmful substances emission into the ecosystem is significantly conserved by the use of cement less concrete [8–13]. In OPC concrete, hydration of constituent material is achieved via reaction of calcium oxide in cement and hydroxide ion in water, however, aluminum-silicate precursors are aiding binding reaction in geopolymer concrete, in a process of geo-polymerization. Among several applications, geopolymer concrete has been incorporated in roller compacted concrete by researchers [14–20], and the studies ascertained the suitability of the materials. While there are numerous investigations on geopolymer concrete [21–24], the current study provides additional insights into the development geopolymer SCC. Enormous benefits can be seen when using SCC for modern day infrastructural development. The use of SCC ensures less energy consumption, labor, and construction cost [25–27].

The development of models for predicting strength characteristics of concrete is continually practiced, to avoid unnecessary repetition of test, and materials wastage. There are popular models like best fit curves (based on regression analysis), which are used for modelling concrete properties. However, due to nonlinearity nature of concrete [28], the models developed using regression analysis may not portray the true nature of the concrete. Also, regression models may not significantly measure the effect of constituent materials in concrete [29].

Artificial neural network (ANN) [30] and genetic programming [31] are some of the recent modeling techniques, which are found applicable to the civil engineering field. These approaches model responses based on incorporated input parameters, and the output models are verified with experimentation. ANN is capable of yielding suitable outputs in situations involving data classification, prediction, optimization and forecasting Parichatprecha and Nimityongskul (2009). For construction applications, GEP and ANN predicts the strength of concrete [29,33–41]; performance of bituminous mixtures [42]; concrete durability [43–45].

Other applications of GEP and ANN have been found in recycled aggregate concrete [46], asphaltic and blast furnace slag [39,47]. Based on the available data in open literature, GEP and ANN demonstrate strong capacity to solve science and engineering problems. Despite the reported cases of modelling geopolymer concrete properties [48–51], the use of GEP and ANN have for predicting properties of geopolymer self-compacting concrete (GSCC) have not been overly explored. This study presents models, developed based on GEP and ANN techniques, predicting strength characteristics of GSCC. These models are expected to fit field applications involving the use of geopolymers.

2. Experimental work

2.1. Materials and method

Low calcium fly ash (ASTM class F), ground granulated blast furnace slag (GGBS) and silica fumes were the pozzolanic materials used. The materials emanate from production of steel, silicon and ferrosilicon. During preparations, the materials were ground onto fine particles, having sizes and specific surface of 16 μm and specific surface of 390 −420 m^2/Kg, respectively. Table 1 shows the chemical oxide compositions of the pozzolans (obtained using X-ray florescence (XRF)). In the experimentation, fly ash was partially replaced (separately) with GGBS and silica fumes in as follows: 10%, 20%, 30%, and 5%, 10%, 15%, respectively.

Granite of 12 mm and reviver sand of sizes lesser than 4.75 mm aperture opening, were used as coarse aggregate and fine aggregate, respectively. The aggregates were preserved in a saturated surface dry (SSD) state, to avoid surface adsorption of moistures, and ensuring adequate bounding of aggregate

Table 1 – Chemical oxide composition of the pozzolans.

Oxides (%)	SiO_2	Al_2O_3	Fe_2O_3	CaO	MgO	Na_2O	K_2O	P_2O_5	SO_3	TiO_2	LOI
Fly ash	49.0	27.25	13.5	1.79	0.89	0.32	0.46	0.98	–	1.54	0.64
GGBS	40.1	9.4	1.2	35.4	4.4	1.7	–	–	–	–	3.1
Silica fume	93.4	0.45	0.87	–	0.84	–	1.7	–	–	–	–

Table 2 – A typical mix proportion for the geopolymer SCC.

Mix	Fly ash (kg/m^3)	Silica fume (kg/m^3)	GGBS (kg/m^3)	River sand (kg/m^3)	Granite (kg/m^3)	NaOH (kg/m^3)	Na_2SiO_3 (kg/m^3)	W/G	Extra Water (%)	SP (%)
GSCC0	450	–	0	850	950	57	143	0.33	12	7
GSCC1	405	–	45	850	950	57	143	0.33	12	7
GSCC2	360	–	90	850	950	57	143	0.33	12	7
GSCC3	270	–	135	850	950	57	143	0.33	12	7
GSCC4	427.5	22.5		850	950	57	143	0.33	12	7
GSCC5	405	45		850	950	57	143	0.33	12	7
GSCC6	382.5	67.5		850	950	57	143	0.33	12	7

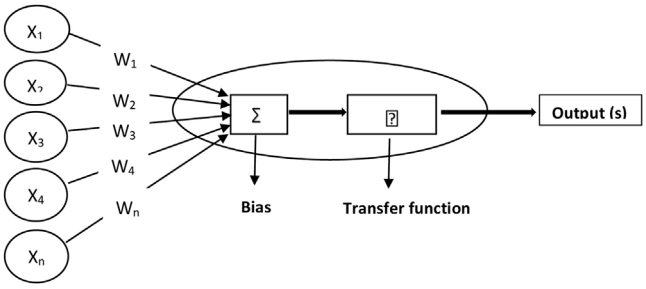

Fig. 1 – Typical ANN model or architecture.

to the paste. This was achieved by initially soaking the aggregates in water, and afterwards air-dried in the laboratory. This helps to dry the surface of the aggregates and interpore water is still present in aggregate. Blocking effect, synonymous with SCC, was prevented by moderately utilizing coarse fractions of aggregate in the mixtures [52]. Also, the approach allows good flow ability of SCC mixtures. Other materials utilized are aggregate, conplast 430 superplasticizer (A modified Polycarboxylate based superplasticizer, of pH value 9.5 at 24 °C), and their properties.

The following properties of the aggregates were determined: specific gravity (SG), water absorption (WA), fineness modulus (FM), bulk density (BD), aggregate crushing value (ACV, and aggregate impact value (AIV). The aggregate properties were determined following standard procedures [53–55], accordingly.

The alkaline solution used for the activation of the pozzolans was composed of NaOH and Na_2SiO_3 solutions, mixed together by Na_2SiO_3/NaOH ratio of 2.5.

2.2. *Sample preparation and testing*

The alkaline solution was prepared a day before use, so as to control temperature rise that occur as a result of polymerization reaction between the two compounds. However, there was need to cool down the alkali activators due to the exothermic reaction that occurs when sodium hydroxide pellets dissolve in water. A procedure to those available in published works [52,56,57] on geopolymers was adopted. As such, this will ensure the generality of use of the models being developed. Table 2 shows the mixes of the geopolymer SCC that were studied. The molarity of NaOH was kept constant at 12 M for all the geopolymer SCC produced, because this concentration of NaOH was reported as adequate for obtaining high strength in geopolymer concrete [52,57,58].

In geopolymer preparation, geopolymer solid or total powder content represent the total mass of fly ash and all other pozzolans. The water to geopolymer solid ratio (W/G) and total powder content were maintained at 0.33 and 450 kg/m^3 respectively.

In SCC, slump is a very important workability test, it reveals the filling ability or passing ability quality of the mixture. In this study, the workability of the SCC mixes was assessed through slump flow, T50 cm, V-funnel, L-box, and J-ring tests. Based on the European Federation of National Associations Representing Producers and Applicators of Specialist Building Products for Concrete EFNARC (2002) classifications, slump flow, T50 cm, and V-funnel tests are for filling ability properties of SCC, while L-box and J-ring tests are for passing ability of SCC.

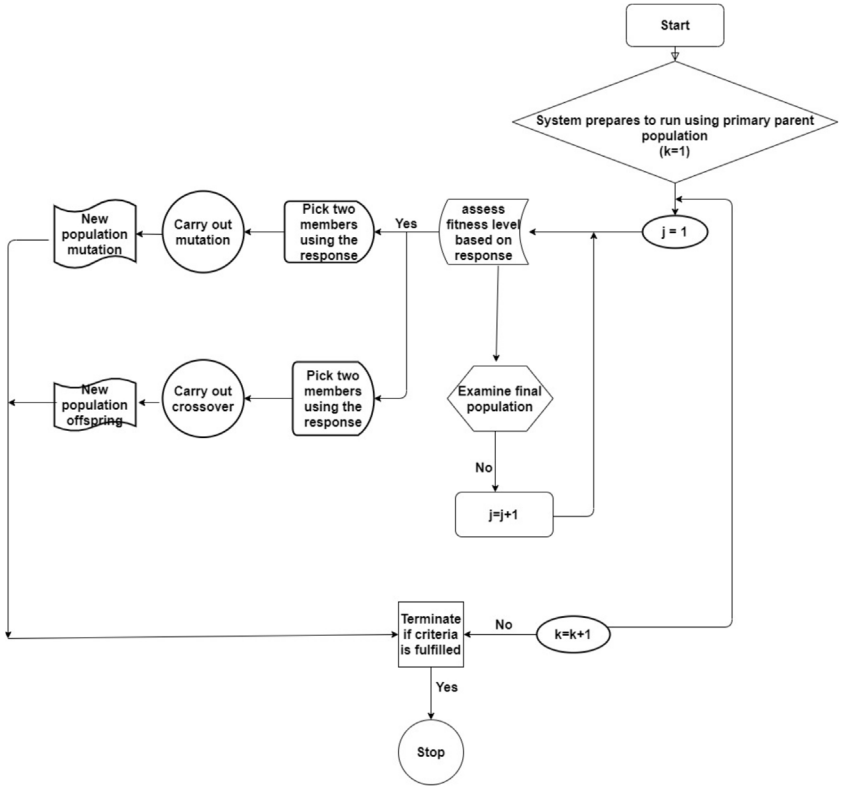

Fig. 2 – GEP operation flowchart.

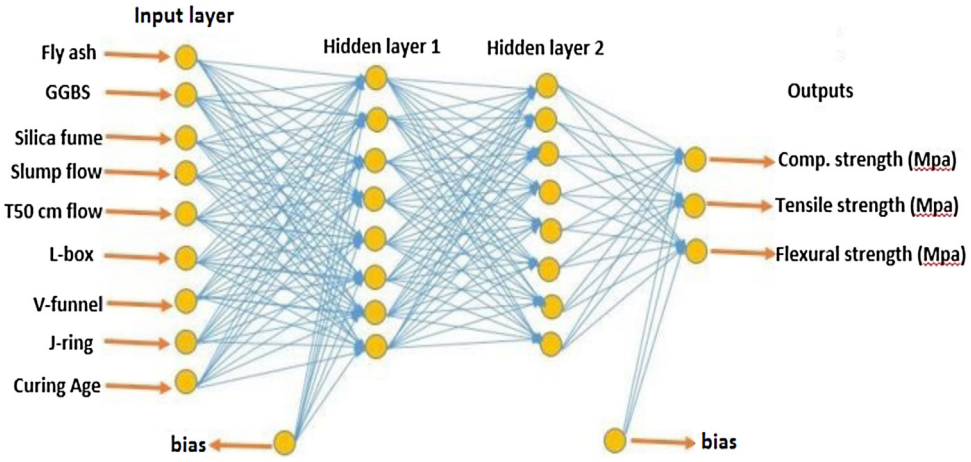

Fig. 3 – ANN architecture that best model the performance of the concrete.

Sample preparation for hardened concrete tests includes 150 mm dimension cubes for compressive strength tests, 100 mm x 200 mm cylinders for split-tensile strength tests, and 100 mm x 100 mm x 500 mm prisms for flexural strength tests. The compressive strength, split-tensile strength, and flexural strength results reported were taken from an average strength of 3, 3, and 2 specimens respectively. A potable water was used for the mixing of the concrete constituents, in line with BS EN, 1997. The GSCC samples were cured in oven constantly at 70 °C for 48 h, normally at this condition, geopolymers strength properties are enhanced. Reports by Nuruddin et al. [57] and Ushaa et al. [52] suggest that a temperature above 70 °C and curing period beyond 48 h could reduce the strength of geopolymers. This approach is practicable, sustainable and economical, mainly because this kind of concrete is best applied in precast plant, where all the required design conditions can be put in place. After the oven curing, the cured in an ambient temperature condition until the test dates of 7, 14 and 28 days. (Figs. 1–3)

3. Modelling concrete strength properties

3.1. *ANN techniques*

The principle of artificial neural network has its relevance in solving diverse problems in science and engineering. It is commonly introduced for developing predictive statistical models for complex processes which are fundamentally nonlinear systems. A number of complex system behavior can be simulated using ANN [61]. The ANN operation is much more like a typical human brain, with components ascribed as neuron. The concept of ANN could also be likened to the way a computer operates, as in "garbage in, garbage out", because it uses input factors to simulate the system process for determination of the output factors. In other words, ANN model development requires input and output components, where the latter is totally influenced by the former [62]. The ANN principle is systematic, in that, the neurons are linked together, and each link possesses its own weight [47]. Thus, the weight multiplied by the transmitted signals in the network gives the solution to the

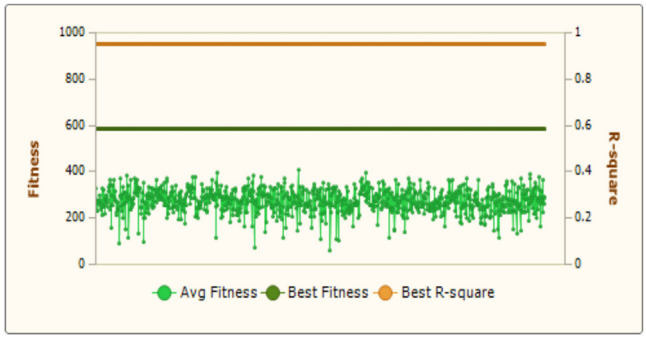

Fig. 4 – Typical dispersion of data during GEP analysis.

model. A typical ANN network architecture comprises of the input layer, hidden layers and the output layer [42]. The input and output layers are predefined before data training, while the hidden layer is determined based on trial and error. A typical ANN architecture model is presented in Fig. 4. The model consists input factors (x_1, x_2, x_3, x_4 ---- x_n), having weights (W_1, W_2, W_3, W_4 ----- W_n), respectively. The remaining processing mechanism is sigmoid or sum function (sigmoid) that finally influences the output(s). Thus, a general description of the analogy is given in Eq. 1,

$$output = \sum_{n=0}^{n} X_n W_n - b \quad (1)$$

Where W_n = weight, and X_n = input, and b = bias.

The potential of the ANN technique to predict meaningful responses has been displayed in studies, irrespective of whether the data being processed are full of errors or maybe incomplete [63,64]. The ANN technique basically comprises of three processes which are learning, training and model performance testing. At the training stage, there is an adjustment of the weights and biases in the network (supervised or unsupervised), so as to accurately determine the output variables. In the supervised training, already completed experimental data are utilized for model development, while the unsupervised training does not use real input and output data.

Table 3 – Input and output data specification for the model development.

Input data	minimum	maximum
Fly ash (kg/m^3)	270	450
GGBS (kg/m^3)	0	135
Silica fume (kg/m^3)	0	67.5
Slump flow (mm)	650	690
T50 cm (s)	3	4.7
L-box	0.88	0.96
V-funnel (s)	9.3	14
J-ring (mm)	3	5.4
Age (days)	7	28
Outputs		
Compressive strength (kN/m^2)	24.67	38.55
Split-tensile strength (kN/m^2)	1.04	4.62
Flexural strength (kN/m^2)	1.03	4.82

At the testing stage, the network will reply to the input without necessarily affecting overall network architecture [42].

At every stage of the ANN construction, a series of trial and error is done, before the best network can be selected. A study by Alshihri has shown that the trial and error process could be prolonged, so as to generate a number of networks, after which the process can be stopped, and tested at different stages of the learning. This process may be repeated by reanalyzing the network using different sets of random weights. Finally, a suitable ANN architecture is the model that possesses the least mean square error (MSE) between the predicted output and actual outputs dataset.

The ANN model development was performance using MATLAB software. The error backpropagation, which adopts training and recall algorithm [65] was used for the model development. According to Lee [62], this approach could solve problems involving multiple variables (multidimensional). The input and output dataset used for model development in this study are presented in Table 3. Feed forward back propagation model, which is based on the Levenberg–Marquardt (LM) multilayer method, available in MATLAB was used for training the data. A data set including 105 data samples obtained from this study and other related experiments were utilized for developing the ANN models. The input data were divided into three parts, seventy percent of the data were used at the learning phase, and fifteen percent each for the testing and validation phases, respectively. As against manual division with maximum values, normalizing of the data was done by default in MATLAB. The process was repeated, based on trial and error, before the suitable model was selected, which satisfied the MSE criteria.

3.2. *GEP techniques*

Gene expression programming (GEP), a subset of genetic algorithm, is a modelling tool developed by Koza [66]. GEP operates as an independent domain for finding solutions to problems or an approximate solution. It was found on the crossover and mutation genetics of Darwinian reproduction and survival principle. GEP can precisely predict the given phenotype of gene sequence (in form of Karva language). A flowchart showing the mode of operation of GEP is presented in Fig. 5.

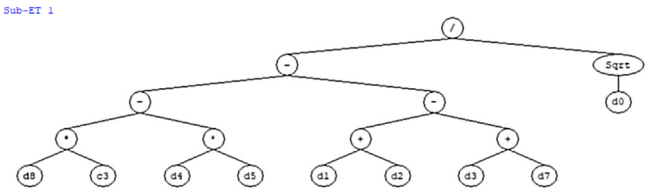

Fig. 5 – Expression tree for compressive strength.

Table 4 – GEP modeling specifications.

Parameter	Parameter description	Parameter setting
k1	Chromosomes	30
k2	Fitness function error type	RMSE
k3	Number of the genes	1
k4	Head size	7
k5	Linking function	Addition
k6	Function set	+, –, ×, /, Exp, Sqrt
k7	Mutation rate	0.00138
k8	One-point recombination	0.00277
k9	Two-point recombination	0.00277
k10	Inversion rate	0.00546
k11	Transposition rate	0.00546

Generally, GEP operates in form of computer program, having varying sizes and shape codes in fixed length linear chromosomes. Thus, the chromosomes are having many genes, and a gene is encoded in form of mini program. The mutation, recombination and transportation of the gene is achieved via its functional and structural organization [67,68].

In this study, the data utilized for the GEP modelling comprised results of the strength tests, and in addition with data soured from literature. Specifications adopted in the GEP operation are presented in Table 4. Modeling in GEP takes the general format as:

$$M_i = \sum_{j=1}^{k_t} \left(F - |K_{(i,j)} - T_j|\right) \tag{2}$$

Where M_i is the fitness function, M is the data selection range, K(i,j) is the value returned by the individual chromosome i for fitness case j (out of K_t fitness cases), and Tj is the target value for fitness case j. If $|K_{(i,j)} - Tj|$ (the precision) $\leqq 0.01$, then the precision = 0, and $Mi = M_{max} = K_tF$. In this study, M was taken 100, and M_{max} is then 1000. This fitness function is capable of generating an optimal solution without any external input.

Altogether, a total of 412 data sets were utilized in the model development, out of which 80% was utilized for training/validation of the GEP model, and 20% of the data set were used for the testing of the model.

$$R = \frac{\sum_{i=1}^{N}(m_i - \overline{m}_i)(p_i - \overline{p}_i)}{\sqrt{\sum_{i=1}^{N}(m_i - \overline{m}_i)^2 \sum_{i=1}^{N}(p_i - \overline{p}_i)^2}} \tag{3}$$

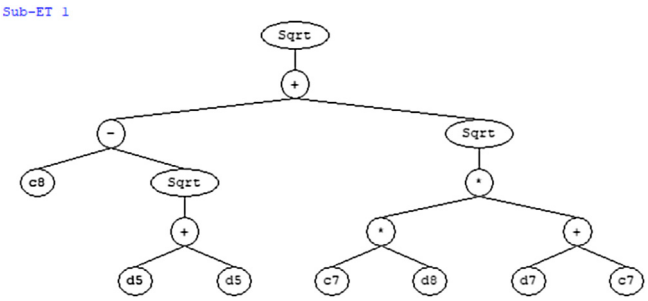

Fig. 6 – Expression tree for split tensile strength.

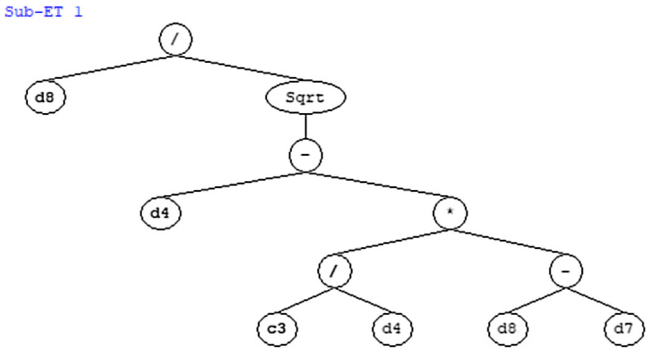

Fig. 7 – Expression tress for flexural strength.

$$RMSE = \sqrt{\frac{1}{N}\sum_{i=1}^{N}(m_i - p_i)^2} \quad (4)$$

$$AAE = \frac{1}{N}\sum_{i=1}^{N}\frac{|m_i - p_i|}{m_i} \times 100 \quad (5)$$

Where N is sample numbers, mi is actual value, pi = predicted value, m_i is the average actual values, and p_i is average predicted values.

Overall, three models were developed for solving compressive strength, split tensile strength and flexural strength of GSCC, respectively.

4. Results and discussion

4.1. *Fresh and hardened properties of the concrete*

Table 5 shows the experimental results of the workability of fresh GSCC, investigated through slump flow, T50 cm flow, L-box test, V-funnel and J-ring tests, and the hardened properties (compressive strength, split-tensile strength and flexural strength). The workability values obtained from the tests were compared with the recommended acceptable limits by EFNARC (2002). As can be seen from the Figures, all the specimens, except specimen without GGBS and silica fume (GSCC0), passed the workability requirements, which thus indicated that the viscosity of the mixtures was adequate. In mix GSCC0, which serves as the control geopolymer, the V-funnel value was higher than the limits recommended (Fig. 6d), this could be attributed to its higher viscosity and segregation [57]. Mainly, two approaches may be considered for controlling the viscosity (flowability) of geopolymers having no GGBS and silica fume, one is to increase superplasticizer contents, and/or increase the extra water [59].

The strength properties of all the tested mixes increased with increasing curing age through 28 days, this kind of performance is a common attribute of an OPC mix. The 28 days strength properties of a geopolymer containing 30% GGBS as replacement of fly ash (GSCC3) was higher than other mixes. The increased admixtures content as replacement of fly ash plays a vital role in reducing the porosity of the matrix, which in turn influenced an increase in the strength properties. In other mixture category, a geopolymer mix containing 10% silica fume as replacement for fly ash (GSCC5) developed the second higher strength properties. However, when silica fume content goes beyond 10%, the strength properties of the mix decreased. The decline in strength properties of the specimens with large silica fume content may be attributed to a slower pozzolanic reaction in the matrix, this significantly affects the rate of hydration as well. There was a measurable increase in strength properties of specimens containing admixtures than control geopolymer specimen, this suggest that admixtures such as GGBS and silica fume are effective for production of GSCC. (Figs. 7,8)

4.2. *ANN modelling results*

A model for predicting the compressive strength, split-tensile strength, and the flexural strength of geopolymer self-compacting concrete was developed, after a series of trial and error. For the type of concrete produced, the input data, which directly affects the concrete performance, were fly ash, GGBS, silica fume, slump flow, T50 cm flow, L-box, V-funnel, J-ring and curing age. While the outputs factors are compressive strength, split tensile strengths, and flexural strength. The output data were the concrete strength parameters obtained at 7, 14, and 28 days testing regimes (age). The ANN architecture that best model the performance of the concrete, and having the lowest error (MSE) value is presented in Fig. 9. There are nine neurons in the input phase, sixteen neurons in the hidden layer and three neurons in the output layer of the model. Table 6 shows the details of correlation and error analysis of the selected model. (Fig. 10)

From results in Table 6, it can be seen that the selected model fulfils the requirement of error performance in ANN model. The model possess R^2 closing to 1 and a smaller MSE, so it is an indication that there exist a perfect strong correlation between the predicted and the actual data. It is known that a good ANN model should possess higher R^2 value or smaller MSE [30], and such model is perfect predicting the behavior of a system. Both the MSE and R^2 were determined based on the following mathematical expressions [39,69]:

$$MSE = \frac{\sum_{i=1}^{n}(o_i - t_i)^2}{n} \quad (6)$$

$$R^2 = \frac{\sum(o - t)^2}{\sum(o - o_{mean})^2} \quad (7)$$

Table 5 – Fresh and hardened properties of geopolymer SCC.

Fly ash	GGBS	Silica fume	Slump flow	T50cm	V-funnel	L-box	J-ring	Age	Compressive strength	Split-tensile strength	Flexural strength
450	0	0	650	4.5	14	0.88	4.5	7	29.11	2.3	2.2
450	0	0	650	4.5	14	0.88	4.5	14	32.89	3.25	3.86
450	0	0	650	4.5	14	0.88	4.5	28	34.67	4.2	4.2
405	45	0	660	4	12	0.94	4	7	28.96	1.78	1.67
405	45	0	660	4	12	0.94	4	14	32.44	3.11	3.71
405	45	0	660	4	12	0.94	4	28	35.92	4.44	4.43
360	90	0	670	4	11.5	0.96	3.5	7	27.74	1.38	1.27
360	90	0	670	4	11.5	0.96	3.5	14	32	2.97	3.5
360	90	0	670	4	11.5	0.96	3.5	28	36.26	4.56	4.63
270	135	0	680	4.5	10.5	0.95	3	7	24.67	1.04	1.03
270	135	0	680	4.5	10.5	0.95	3	14	31.11	2.83	3.26
270	135	0	680	4.5	10.5	0.95	3	28	38.55	4.62	4.82
427.5	0	22.5	660	3	9.3	0.89	5	7	31.66	2.82	2.82
427.5	0	22.5	660	3	9.3	0.89	5	14	33.33	3.51	4.1
427.5	0	22.5	660	3	9.3	0.89	5	28	36	4.2	4.28
405	0	45	680	3.5	9.5	0.92	5	7	30.74	3.32	3.27
405	0	45	680	3.5	9.5	0.92	5	14	35.56	3.88	4.4
405	0	45	680	3.5	9.5	0.92	5	28	37.38	4.44	4.6
382.5	0	67.5	690	4.7	11	0.96	5.4	7	31	2.86	2.86
382.5	0	67.5	690	4.7	11	0.96	5.4	14	33.78	3.62	4.2
382.5	0	67.5	690	4.7	11	0.96	5.4	28	35.56	4.38	4.3

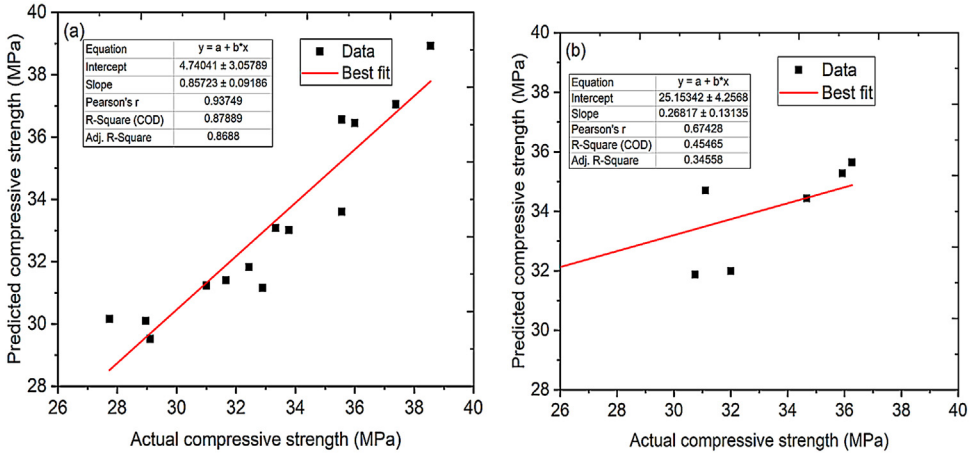

Fig. 8 – Compressive strength (a) Train data set (b) Test data set.

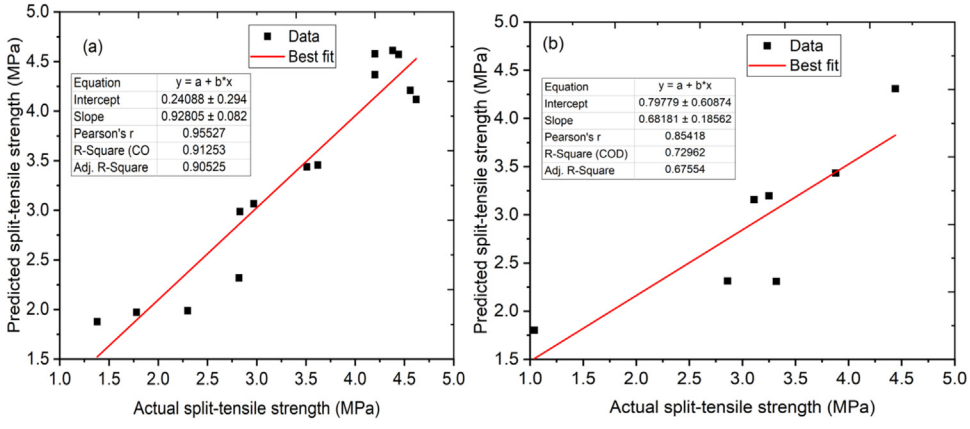

Fig. 9 – Split-tensile strength (a) Train data set (b) Test data set.

Table 6 – Correlation and error analysis of the ANN model selected.

Final Model	Training		Test		Validation	
	MSE	R^2	MSE	R^2	MSE	R^2
9–8-8–3	0.00603	0.97	0.00566	0.89	0.00564	0.96

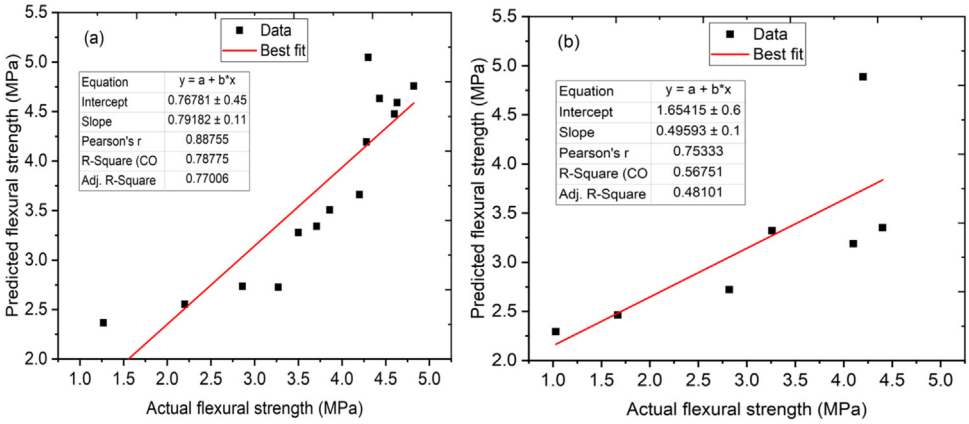

Fig. 10 – Flexural strength (a) Train data set (b) Test data set.

where n is the total data number, o is the output, t is the target output, and o_{mean} is the average value of the network output.

Based on the performance of the selected network architecture, thus, it is clear that there exists strong agreement between the predicted data and actual experimental data obtained on GSCC. The selected model has capability to generalize both input and output data of the tested concrete with a high level of accuracy in the predictions. In addition, another fact that backs the section of this model is that it has a minimal corresponding percent error for the predicted strength, and in statistical term, the prediction with this model can be reliable. This result shows there is absolute reliability in the model performance, because of closeness of the datasets (predicted and actual). Overall, it is an indication that the selected model can produce accurate response for a system with a strong confidence level.

4.3. *GEP model results*

This study developed three models for each of the GSCC strength parameter investigated. Similar predictor and responses used in the ANN model were also utilised for the GEP model. A typical dispersion of data during GEP analysis is shown in Fig. 11. Models for the responses were obtained by reading the expression trees, bottom left to the right side.

Model expression trees for the compressive strength, split tensile strength and flexural strength are shown in Figs. 12–14, respectively. Also, comparison between predicted and the actual experimental data (train and test/validation datasets), for compressive strength, split tensile strength and flexural strength are shown in Figs. 15–17, respectively. From these Figures, it can be seen that there is a good correlation between the model prediction and the actual experimental data. This thus shows the adequacy of the model for

Fig. 11 – Typical dispersion of data during GEP analysis.

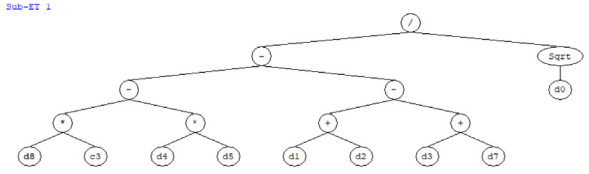

Fig. 12 – Expression tress for compressive strength.

further applications. Based on the error values presented for compressive strength, split tensile strength and flexural strength in Tables 7–9, respectively, it is shown that R values were more than 0.64 limit [70], therefore the model can be adjudged suitable for application in the geopolymer concrete.

In formulating expressions for compressive strength, split tensile strength and flexural strength, using the expression trees, the following notations were adopted:

Cs = compressive strength, Ss = Split-tensile strength, Fs = flexural strength, F = fly ash, T50 = T50 flow, V = V funnel flow, Sf = Silica fume, S = slump flow, J = J-ring, A = Age, L = L-box, G = GGBS

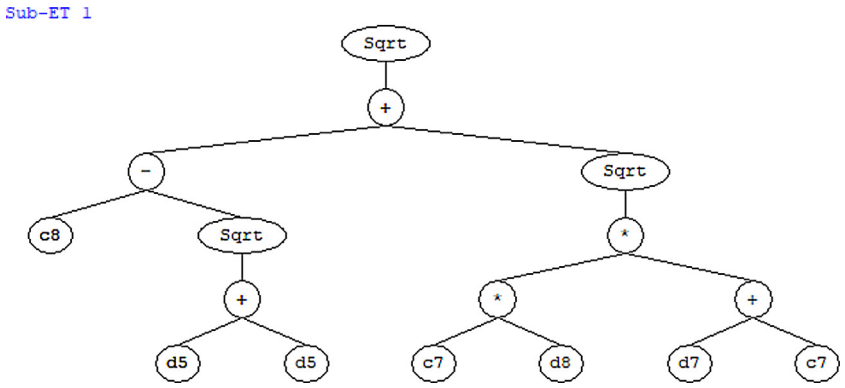

Fig. 13 – Expression tress for split tensile strength.

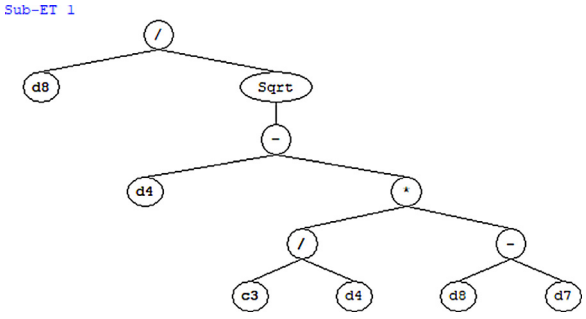

Fig. 14 – Expression tress for compressive strength.

The developed models for compressive strength, split tensile strength and flexural strength are presented as follows:

$$Cs = \frac{1}{\sqrt{F}}(4.96A - (T_{50}V)) - (G + S_f) - (S + J) \quad (8)$$

$$Ss = ((V - 5.88) + (\sqrt{(15.13AJ)})^{\frac{1}{2}} \quad (9)$$

$$Fs = \frac{A}{\sqrt{T_{50} + \frac{5.42}{T_{50}}(A - J)}} \quad (10)$$

5. Conclusion

This study focuses on modelling the strength properties of GSCC containing mineral admixtures, using genetic programming and artificial neural networks. The following conclusions were drawn from the study:

1 From the assessment of GSCC fresh properties, results showed that the samples prepared with mineral admixtures satisfied the EFNARC limits. The control mixture (made of conventional material) also met the requirements, except that V-funnel result exceed limit of 12 s set by the standard. Such performance could be a result of high viscosity and segregation of the mixture.

2 There was increase in strength properties of all samples with increasing curing regimes, and generally, samples prepared with mineral admixtures developed strengths comparable to the control mixture.

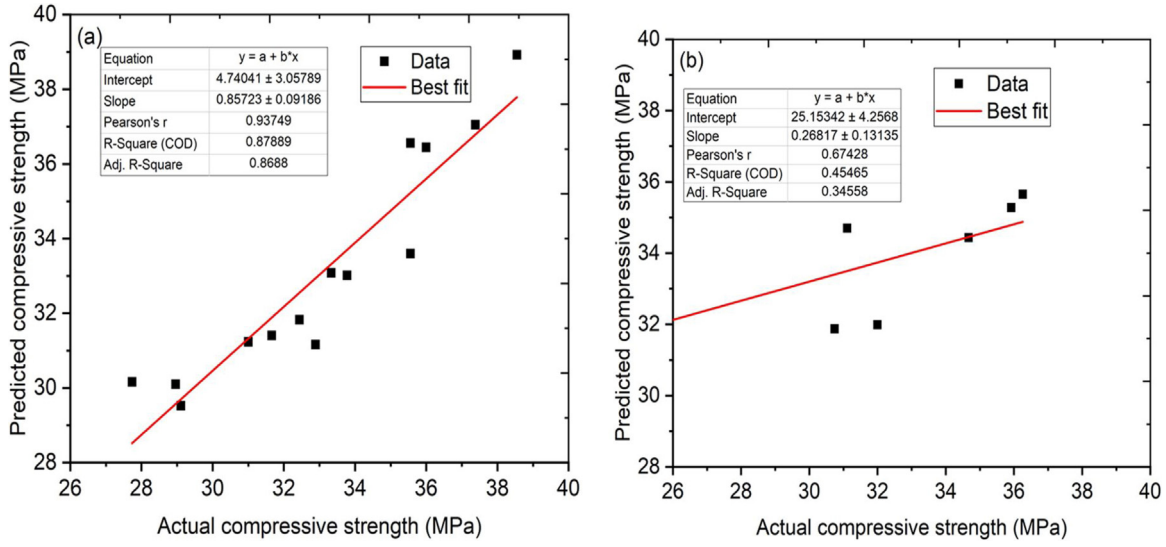

Fig. 15 – Compressive strength (a) Train data set (b) Test data set.

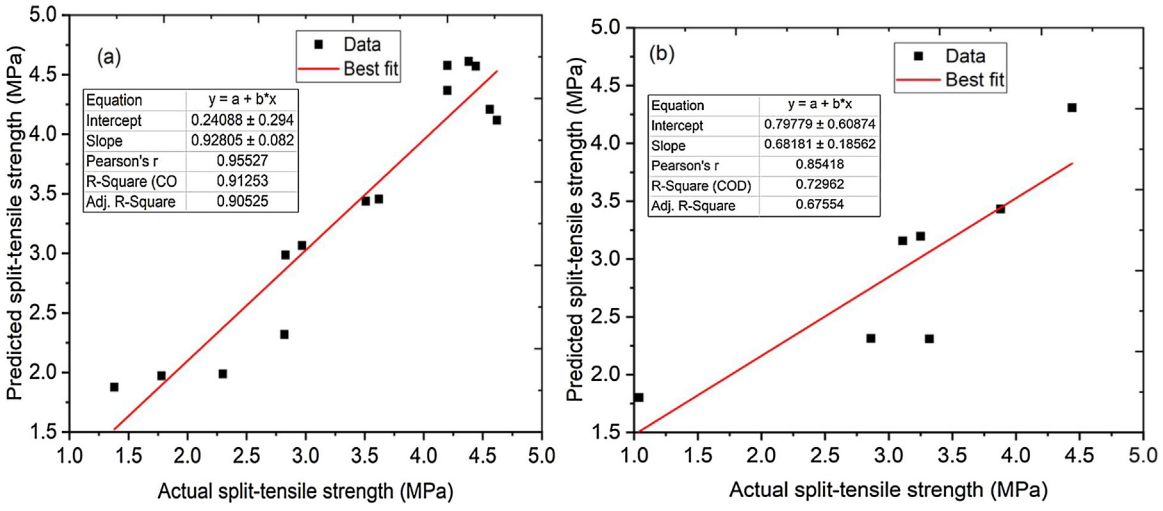

Fig. 16 – Split-tensile strength (a) Train data set (b) Test data set.

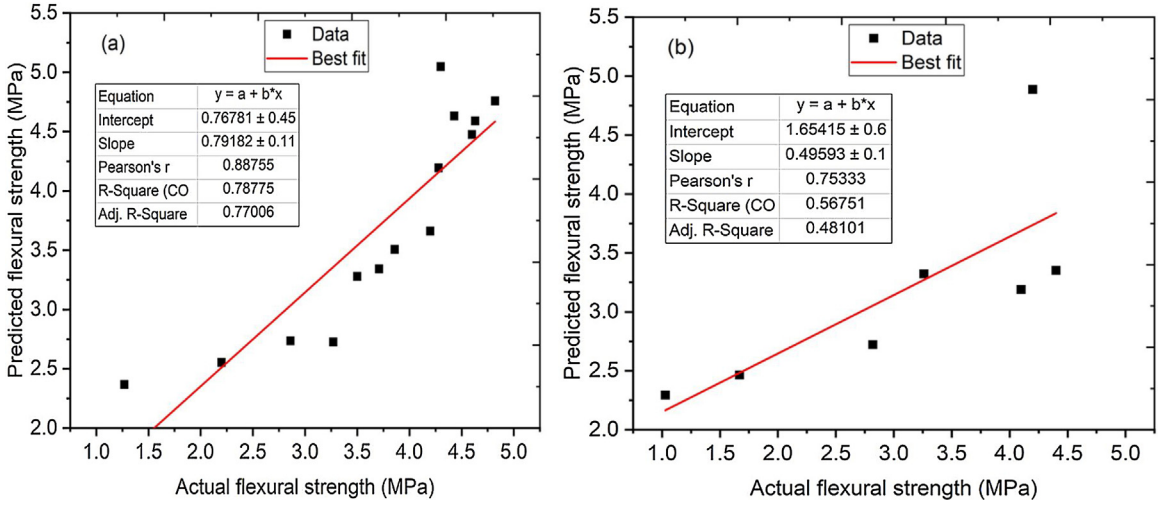

Fig. 17 – Flexural strength (a) Train data set (b) Test data set.

Table 7 – Statistical data: compressive strength.

Index	Train data	Test data
RMSE	1.09	3.33
MSE	1.19	11.10
MAE	0.85	2.02

3 In the model developed using GEP and ANN, it has been shown that both the predicted data and actual experimental dataset possess significant uniqueness. The results of compressive strength, split-tensile strength and flexural strength have been compared based on the values of MSE and R^2. It is thus clear that the GEP and ANN models developed for the GSCC are reliable, and have the capacity to measure the concrete properties at somewhat 97% confidence level. Overall, GEP model is preferred as it gives mathematical expression for solving the investigated strength parameters.

Table 8 – Statistical data: split-tensile strength.

Index	Train data	Test data
RMSE	0.30	0.55
MSE	0.09	0.30
MAE	0.26	0.42

Table 9 – Statistical data: flexural strength.

Index	Train data	Test data
RMSE	0.45	0.81
MSE	0.20	0.66
MAE	0.34	0.69

Conflict of interest

The authors declared that there are no conflict of interest.

REFERENCES

[1] Hardjito D, Wallah S, Sumajouw D, Rangan B. Factors influencing the compressive strength of fly ash-based geopolymer concrete. Civ Eng Dimens 2004;6:88–93.

[2] Rangan B. Fly ash-based geopolymer concrete. Curtin Univ Technol Perth 2008.

[3] Oliveira MLS, Izquierdo M, Querol X, Lieberman RN, Saikia BK, Silva LFO. Nanoparticles from construction wastes: a problem to health and the environment. J Clean Prod 2019;219:236–43, http://dx.doi.org/10.1016/j.jclepro.2019.02.096.

[4] Oliveira MLS, Tutikian BF, Milanes C, Silva LFO. Atmospheric contaminations and bad conservation effects in Roman mosaics and mortars of Italica. J Clean Prod 2020;248:119250, http://dx.doi.org/10.1016/j.jclepro.2019.119250.

[5] MM A, Tutikian BF, Ortolan V, Oliveira MLS, Sampaio CH, Gómez PL, et al. Fire resistance performance of concrete-PVC panels with polyvinyl chloride (PVC) stay in place (SIP) formwork. J Mater Res Technol 2019;8:4094–107, http://dx.doi.org/10.1016/j.jmrt.2019.07.018.

[6] Gómez-Plata L, Tutikian BF, Pacheco F, Oliveira MS, Murillo M, Silva LFO, et al. Multianalytical approach of stay-in-place polyvinyl chloride formwork concrete exposed to high temperatures. J Mater Res Technol 2020, http://dx.doi.org/10.1016/j.jmrt.2020.03.022.

[7] Sathanandam T, Awoyera PO, Vijayan V, Sathishkumar K. Low carbon building: experimental insight on the use of fly ash and glass fibre for making geopolymer concrete. Sustain Environ Res 2017;27:146–53, http://dx.doi.org/10.1016/j.serj.2017.03.005.

[8] Gallego-Cartagena E, Morillas H, Maguregui M, Patiño-Camelo K, Marcaida I, Morgado-Gamero W, et al. A comprehensive study of biofilms growing on the built heritage of a Caribbean industrial city in correlation with construction materials. Int Biodeterior Biodegradation 2020;147:104874, http://dx.doi.org/10.1016/j.ibiod.2019.104874.

[9] Silva LFO, Pinto D, Neckel A, Dotto GL, Oliveira MLS. The impact of air pollution on the rate of degradation of the fortress of Florianópolis Island. Brazil. Chemosphere 2020;251:126838, http://dx.doi.org/10.1016/j.chemosphere.2020.126838.

[10] Silva LFO, Pinto D, Neckel A, Oliveira MLS, Sampaio CH. Atmospheric nanocompounds on Lanzarote Island: vehicular exhaust and igneous geologic formation interactions. Chemosphere 2020;254:126822, http://dx.doi.org/10.1016/j.chemosphere.2020.126822.

[11] Morillas H, García-Florentino C, Marcaida I, Maguregui M, Arana G, Silva LFO, et al. In-situ analytical study of bricks exposed to marine environment using hand-held X-ray fluorescence spectrometry and related laboratory techniques. Spectrochim Acta Part B At Spectrosc 2018;1(46):28–35, http://dx.doi.org/10.1016/j.sab.2018.04.020.

[12] Morillas H, Vazquez P, Maguregui M, Marcaida I, Silva LFO. Composition and porosity study of original and restoration materials included in a coastal historical construction. Constr Build Mater 2018;178:384–92, http://dx.doi.org/10.1016/j.conbuildmat.2018.05.168.

[13] Morillas H, Maguregui M, Gallego-Cartagena E, Huallparimachi G, Marcaida I, Salcedo I, et al. Evaluation of the role of biocolonizations in the conservation state of Machu Picchu (Peru): the Sacred Rock. Sci Total Environ 2019;654:1379–88, http://dx.doi.org/10.1016/j.scitotenv.2018.11.299.

[14] Castel A, Foster SJ. Bond strength between blended slag and Class F fly ash geopolymer concrete with steel reinforcement. Cem Concr Res 2015;72:48–53, http://dx.doi.org/10.1016/j.cemconres.2015.02.016.

[15] Reed M, Lokuge W, Karunasena W. Fibre-reinforced geopolymer concrete with ambient curing for in situ applications. J Mater Sci 2014;49:4297–304, http://dx.doi.org/10.1007/s10853-014-8125-3.

[16] Singh B, Ishwarya G, Gupta M, Bhattacharyya SK. Geopolymer concrete: a review of some recent developments. Constr Build Mater 2015;85:78–90, http://dx.doi.org/10.1016/j.conbuildmat.2015.03.036.

[17] Part WK, Ramli M, Cheah CB. An overview on the influence of various factors on the properties of geopolymer concrete derived from industrial by-products. Constr Build Mater 2015;77:370–95, http://dx.doi.org/10.1016/j.conbuildmat.2014.12.065.

[18] Heah CY, Kamarudin H, Mustafa Al Bakri AM, Binhussain M, Luqman M, Khairul Nizar I, et al. Effect of curing profile on kaolin-based geopolymers. Phys Procedia 2011;22:305–11, http://dx.doi.org/10.1016/j.phpro.2011.11.048.

[19] Nagalia G, Park Y, Ph D, Asce M, Abolmaali A, Ph D, et al. Compressive strength and microstructural properties of fly ash – based geopolymer concrete. J Mater Civ Eng 2016:1–11, http://dx.doi.org/10.1061/(ASCE)MT.1943-5533.0001656.

[20] Nematollahi B, Sanjayan J, Chai JXH, Lu TM. Properties of fresh and hardened glass Fiber reinforced fly ash based geopolymer concrete. Key Eng Mater 2014;594–595:629–33, http://dx.doi.org/10.4028/www.scientific.net/KEM.594-595.629.

[21] Santana HA, Andrade Neto JS, Amorim NS Junior, Ribeiro DV, Cilla MS, Dias CMR. Self-compacting geopolymer mixture: dosing based on statistical mixture design and simultaneous optimization. Constr Build Mater 2020;249:118677, http://dx.doi.org/10.1016/j.conbuildmat.2020.118677.

[22] Demie S, Nuruddin MF, Shafiq N. Effects of micro-structure characteristics of interfacial transition zone on the compressive strength of self-compacting geopolymer concrete. Constr Build Mater 2013;41:91–8, http://dx.doi.org/10.1016/j.conbuildmat.2012.11.067.

[23] Memon FA, Nuruddin MF, Shafiq N. Effect of silica fume on the fresh and hardened properties of fly ash-based self-compacting geopolymer concrete. Int J Miner Metall Mater 2013;20:205–13, http://dx.doi.org/10.1007/s12613-013-0714-7.

[24] Nuruddin MF, Demie S, Shafiq N. Effect of mix composition on workability and compressive strength of self-compacting geopolymer concrete. Am J Civ Eng Archit 2011;38:1196–203, http://dx.doi.org/10.1139/l11-077.

[25] Karthika V, Awoyera PO, Akinwumi II, Gobinath R, Gunasekaran R, Lokesh N. Structural properties of lightweight self-compacting concrete made with pumice stone and mineral admixtures. Rev Rom Mater Rom J Mater 2018;48.

[26] Palanisamy M, Poongodi K, Awoyera PO, Ravindran G. Permeability properties of lightweight self-consolidating concrete made with coconut shell aggregate. Integr Med Res 2020, http://dx.doi.org/10.1016/j.jmrt.2020.01.092.

[27] Adesina A, Awoyera P. Overview of trends in the application of waste materials in self-compacting concrete production. SN Appl Sci 2019, http://dx.doi.org/10.1007/s42452-019-1012-4.

[28] Awoyera P. Nonlinear finite element analysis of steel fibre-reinforced concrete beam under static loading. J Eng Sci Technol 2016;11:1–9.

[29] Sadrmomtazia A, Sobhanib J, Mirgozar M. Modeling compressive strength of EPS lightweight concrete using regression, neural network and ANFIS. Constr Build Mater 2013;42:205–16.

[30] Zhang G, Patuwo BE, Hu MY. Forecasting with artificial neural networks: The state of the art. Int J Forecast 1998;14:35–62.

[31] Mansouri I, Azmathulla HM, Hu JW. Gene expression programming application for prediction of ultimate axial strain of FRP-confined concrete. Electron J Fac Civ Eng Osijek-e-GFOS 2018;16:64–76.
[33] Topc B. Prediction of compressive strength of concrete containing fly ash using artificial neural networks and fuzzy logic. Computational Material Science 2008;41:305–11, http://dx.doi.org/10.1016/j.commatsci.2007.04.009.
[34] Bhatti MA. Predicting the compressive strength and slump of high strength concrete using neural network. Construction and Building Material 2006;20:769–75, http://dx.doi.org/10.1016/j.conbuildmat.2005.01.054.
[35] Sarıdemir M. Predicting the compressive strength of mortars containing metakaolin by artificial neural networks and fuzzy logic. Adv Eng Softw 2009;40:920–7, http://dx.doi.org/10.1016/j.advengsoft.2008.12.008.
[36] Hong-guang N, Ji-zong W. Prediction of compressive strength of concrete by neural networks. xxx 2000;30:1245–50.
[37] Sobhani J, Najimi M, Pourkhorshidi AR, Parhizkar T. Prediction of the compressive strength of no-slump concrete: A comparative study of regression, neural network and ANFIS models. Constr Build Mater 2010;24:709–18, http://dx.doi.org/10.1016/j.conbuildmat.2009.10.037.
[38] Garzón-roca J, Marco CO, Adam JM. Compressive strength of masonry made of clay bricks and cement mortar: Estimation based on Neural Networks and Fuzzy Logic. Eng Struct 2013;48:21–7, http://dx.doi.org/10.1016/j.engstruct.2012.09.029.
[39] Chen L. Grey and neural network prediction of concrete compressive strength using physical properties of electric arc furnace oxidizing slag. J Environ Eng Manag 2010;20:189–94.
[40] Awoyera PO, Akinmusuru JO, Krishna AS, Gobinath R, Arunkumar B, Sangeetha G. Model Development for Strength Properties of Laterized Concrete Using Artificial Neural Network Principles. Soft Comput Probl Solving Adv Intell Syst Comput 2018;1:197–207, http://dx.doi.org/10.1007/978-981-15-0035-0_15.
[41] Arun Kumar B, Sangeetha G, Srinivas A, Awoyera P, Gobinath R, Venkata Raman V. Models for predictions of mechanical properties of low-density self-compacting concrete prepared from mineral admixtures and pumice stone. Adv Intell Syst Computnd 2019.
[42] Shafabakhsh G, Jafari Ani O, Talebsafa M. Artificial neural network modeling (ANN) for predicting rutting performance of nano- modified hot-mix asphalt mixtures containing steel slag aggregates. Constr Build Mater J 2015;85:136–43, http://dx.doi.org/10.1016/j.conbuildmat.2015.03.060.
[43] Hodhod O, Ahmed HI, Hodhod OA, Ahmed HI. Modeling the corrosion initiation time of slag concrete using the artificial neural network modeling the corrosion initiation time of slag concrete using the artificial neural network. Hbrc J 2014:8–12, http://dx.doi.org/10.1016/j.hbrcj.2013.12.002.
[44] Carmichael RP. Relationships between young's modulus, compressive strength, poisson's ratio, and time for early age concrete 2009; 2020.
[45] Bal L, Buyle-bodin F. Artificial neural network for predicting drying shrinkage of concrete. Constr Build Mater 2013;38:248–54, http://dx.doi.org/10.1016/j.conbuildmat.2012.08.043.
[46] Duan Z, Kou S, Poon C. Prediction of compressive strength of recycled aggregate concrete using artificial neural networks. Constr Build Mater 2013;40:1200–6.
[47] Bilim C, Atis CD, Tanyildizi H, Karahan O. Advances in engineering software predicting the compressive strength of ground granulated blast furnace slag concrete using artificial neural network, 40; 2009. p. 334–40, http://dx.doi.org/10.1016/j.advengsoft.2008.05.005.
[48] Barbuta M, Diaconescu R, Harja M. Using neural networks for prediction of properties of polymer concrete with fly ash. J Mater Civ Eng 2012;24:523–8, http://dx.doi.org/10.1061/(ASCE)MT.1943-5533.0000413.
[49] Nazari A, Torgal FP. Predicting compressive strength of different geopolymers by artificial neural networks. Ceram Int 2013;39:2247–57, http://dx.doi.org/10.1016/j.ceramint.2012.08.070.
[50] Yadollahi MM, Benli A, Demirboğa R. Prediction of compressive strength of geopolymer composites using an artificial neural network Prediction of compressive strength of geopolymer composites using an artificial neural network. Mater Res Innov 2016;19:453–8, http://dx.doi.org/10.1179/1433075X15Y.0000000020.
[51] Nazari A. Artificial neural networks application to predict the compressive damage of lightweight geopolymer. Neural Comput Appl 2013;23:507–18, http://dx.doi.org/10.1007/s00521-012-0945-y.
[52] Ushaa T, Anuradha R, Venkatasubramani G. Performance of self-compacting geopolymer concrete containing different mineral edmixtures. Indian J Eng Mater Sci 2015;22:473–81.
[53] BS 882. Aggregates from natural sources; 1992. Br Stand London, UK.
[54] BS 812-110. Methods for determination of aggregate crushing value (ACV); 1990. Br Stand London, UK.
[55] BS EN 1097-6. Tests for mechanical and physical properties of aggregates; 1995. Br Stand London, UK.
[56] Sashidhar C, Guru Jawahar J, Neelima C, Pavan Kumar D. Preliminary studies on self compacting geopolymer concrete using manufactured sand. Asian J Civ Eng 2016;17:277–88.
[57] Nuruddin M, Demie S, Shafiq N. Effect of mix composition on workabilit. . .of self-compacting geopolymer concrete.pDf. Can. J Civ Eng 2011;38:1196–203.
[58] Fareed A, Muhd F, Sadaqatullah K, Nasir S, Tehmina A. Effect of sodium hydroxide concentration on fresh properties and compressive strength of self-compacting geopolymer concrete. J Eng Sci Technol 2013;8:44–56.
[59] EFNARC. Specification and guildelines for self-compacting conrete; 2002.
[61] Alshihri MM, Azmy AM, El-bisy MS. Neural networks for predicting compressive strength of structural light weight concrete. Constr Build Mater 2009;23:2214–9, http://dx.doi.org/10.1016/j.conbuildmat.2008.12.003.
[62] Lee S. Prediction of concrete strength using artificial neural networks. xxx 2003;25:849–57, http://dx.doi.org/10.1016/S0141-0296(03)00004-X.
[63] Pala M, Özbay E, Öztas A, Yüce M. Appraisal of long-term effects of fly ash and silica fume on compressive strength of concrete by neural networks. Constr Build Mater 2007;21:384–94.
[64] Sangeetha G., Arun Kumar B., Srinivas A., Gobinath R., Awoyera P. Optimization of drilling rig hydraulics in drilling operations using soft computing techniques. Adv Intell Syst Comput n.d.
[65] Zurada J. Introduction to artificial neural systems. Info Access Distrib Ltd; 1992.
[66] Koza JR. Genetic programming: on the programming of computers by means of natural selection; 1992.
[67] Liu SW, Huang JH, Sung JC, Lee CC. Detection of cracks using neural networks and computational mechanics. Comput Methods Appl Mech Eng 2002;191:2831–45, http://dx.doi.org/10.1016/S0045-7825(02)00221-9.
[68] Nazari A. RETRACTED ARTICLE: application of gene expression programming to predict the compressive damage of lightweight aluminosilicate geopolymer. Neural Comput Appl 2019;31:767–76, http://dx.doi.org/10.1007/s00521-012-1137-5.

[69] Tanyildizi H, Özcan F, Atis CD, Karahan O, Uncuog E. Comparison of artificial neural network and fuzzy logic models for prediction of long-term compressive strength of silica fume concrete. Adv Eng Softw 2009;40:856–63, http://dx.doi.org/10.1016/j.advengsoft.2009.01.005.

[70] Farzampour A, Mansouri I, Mortazavi SJ, Hu JW. Force-displacement relationship of a butterfly-shaped beams based on gene expression programming. Korea: 10th Int. Symp. Steel Struct., Jeju; 2019. p. 10–3.